International Journal of Heat and Fluid Flow 29 (2008) 945–956

Contents lists available at ScienceDirect

International Journal of Heat and Fluid Flow

journal homepage: www.elsevier.com/locate/ijhff

An experimental study on hot round jets impinging a concave surface

M. Fenot *, E. Dorignac, J.-J. Vullierme

Laboratoire d'Etudes Thermiques (UMR 6608), 1 Avenue Clement Ader, BP 40109 86961 Futuroscope Chasseneuil Cedex, France

ARTICLE INFO

Article history:
Received 12 September 2007
Received in revised form 25 March 2008
Accepted 27 March 2008
Available online 15 May 2008

Keywords:
Impingement
Hot jets
Curved surface
Thermography

ABSTRACT

An experimental investigation of heat transfer due to a row of air jets impinging on a concave semi-cylindrical surface is presented. Heat transfer characteristics are measured using a heat thin foil technique and infrared thermography. Adiabatic wall temperatures and local heat transfer coefficients are determined by means of a linear regression method. The effect of high relative curvature (d/D) is investigated by changing the jet tube diameter (impinging surface diameter remaining constant). Reynolds number, injection temperature, spacing between adjacent jets and jet exit to surface spacing are also made to vary. Curvature has different effects over the adiabatic wall temperature and Nusselt number distributions. First, the curvature increase provokes a small growth of Nusselt number in the impingement region. On the other hand, curvature produces a confinement of the jet's flow that has two consequences: stagnation of the adiabatic wall temperature and decrease of Nusselt number distribution.

1. Introduction

Jet impingement technique is used in many applications where extensive cooling or heating is necessary on account of its ability to produce a high heat transfer rate in a localised region. These applications include glass production, drying of textile and papers, annealing of metals, and cooling of electronics components. Impinging jets are also used for the cooling of particular regions of turbojet engines where thermal conditions are the most severe: combustion chamber walls and the leading edge of turbine blades. In this last case, jet impingement is used as an internal cooling technique. So, jet impingements on a high relative concave surface and curvature effect should be taken into account when considering heat transfer. Moreover, jet temperature is different from that of the environment in which it is issuing. In this case, entrainment of the surrounding fluid into the jet can greatly affect jet temperature and consequently heat transfer from the impingement surface to the jet.

Many studies have analysed the flow characteristics and heat transfer of one or more impinging jets. Martin (1977), Downs and James (1987), Jambunathan et al. (1992) and Viskanta (1993) referred to a large panel of fundamental studies and presented a complete review on the main parameters influencing heat transfer. Most of these focus on cold jet ($T_j = T_\infty$) impinging on flat plate.

By contrast, relatively few works have been published on impingement over a concave plate. Some of the earliest are those of Metzger et al. (1969), who measured the average heat transfer coefficient due to an array of round jet impinging on a concave surface. Hrycak (1981) mainly studied heat transfer at stagnation point from concave hemispherical plates with small relative curvatures from 0.034 to 0.1 and Reynolds numbers from 12,000 to 88,000.

Some authors have studied impingement of a slot jet on cylindrical surface. Gau and Chung (1991) presented flow visualisations and heat transfer coefficient due to a slot jet impinging on both convex and concave surfaces. Reynolds numbers varied from 6000 to 35,000 and slot width to surface diameter ratios were small (from 0.022 to 0.125). They suggested formation of Taylor–Gortler vortices that enhanced heat transfer but their visualisations failed to confirm this hypothesis. Yang et al. (1999) and Eren et al. (2006) investigated a similar configuration but without relative curvature variation. Gilard and Brizzi (2005) performed flow visualisations and PIV measurements for a slot jet with high relative curvature ($d/D = 0.106–0.192$) and $Re = 1400–3200$. They observed a jet beating phenomenon and a "dead fluid" area near the impingement.

Few articles have dealt with heat transfer from 3D jets (round, square or elliptical jets) impinging on concave surfaces. Flow visualisations and heat transfer from a line of square and elliptic jets with high Reynolds numbers ($Re = 60{,}000–135{,}000$) on concave and convex surfaces with small curvature ($d/D = 0.0197–0.0394$) were studied by Kornblum and Goldstein (1997). This work mainly showed recirculation of the flow exiting the concave surface into the free jet. Lee et al. (1999) studied local heat transfer from a concave surface ($d/D = 0.034–0.09$) with a round jet ($Re = 11{,}000–50{,}000$). The effect of relative curvature is investigated showing that Nusselt number at stagnation point is heightened with increasing values of curvature.

* Corresponding author. Tel.: +33 05 49 49 81 09; fax: +33 05 49 49 81 01.
E-mail address: fenot@let.ensma.fr (M. Fenot).

0142-727X/$ - see front matter © 2008 Elsevier Inc. All rights reserved.
doi:10.1016/j.ijheatfluidflow.2008.03.015

Nomenclature

C_r	relative curvature = d/D
d	jet diameter (m)
D	curved surface diameter (m)
e	impingement plate thickness (m)
H	jet exit to impingement plate distance (m)
h	heat transfer coefficient on front side (W m^{-2} K^{-1})
h_r	heat transfer coefficient on rear side (W m^{-2} K^{-1})
L	tubes length (m)
Nu	Nusselt number = hd/λ_{air}
Nu_{st}	Nusselt number at stagnation point
$\overline{Nu}(s)$	average Nusselt number along Y axis $\left(\overline{Nu}(s) = \frac{1}{P/2}\int_0^{P/2} \times Nu(s,Y)\,dy\right)$
$\overline{\overline{Nu}}$	average Nusselt number for $0 \leqslant Y \leqslant P/2$ and $0 \leqslant s \leqslant 5d$
P	jet center to center spacing (m)
r^2	correlation coefficient of linear regression
Re	Reynolds number = $\rho Vd/\mu$
T_{aw}	adiabatic wall temperature (K)
T_j	injection wall temperature (K)
T_w	front wall temperature (K)
$T_{w,r}$	rear wall temperature (K)
t_∞	ambient temperature (K)
s	curvilinear abscissa from the center of the jets row (m)
Y	spanwise coordinate from the central jet of the row (m)
Z	coordinate from the impingement plate (m)

Greek symbols

ε_w	impingement wall emissivity
η	effectiveness = $(T_{aw} - T_\infty)/(T_j - T_\infty)$
η_{st}	effectiveness at stagnation point
$\overline{\eta}(s)$	average effectiveness along Y axis $\left(\overline{\eta}(s) = \frac{1}{P/2}\int_0^{P/2} \eta \times (s,Y)\,dy\right)$
$\overline{\overline{\eta}}$	average effectiveness for $0 \leqslant Y \leqslant P/2$ and $0 \leqslant s \leqslant 5d$
λ_{air}	air thermal conductivity (W m^{-1} K^{-1})
λ_w	wall thermal conductivity (W m^{-1} K^{-1})
μ_{air}	air dynamic viscosity (N s m^{-2})
ρ_{air}	air density (kg m^{-3})
σ	Stefan–Boltzmann constant = 5.67×10^{-8} (W m^{-2} K^{-4})
φ_{co}	convective heat flux density on the front side (W m^{-2})
$\varphi_{co,r}$	convective heat flux density on the rear side (W m^{-2})
φ_{elec}	electrical flux density dissipated by Joule effect (W m^{-2})
$\varphi_{ra,f}$	radiative heat flux density on the front side (W m^{-2})
$\varphi_{ra,r}$	radiative heat flux density on the rear side (W m^{-2})

Cornaro et al. (1999) examined concave and convex surface with high relative curvature from 0.18 to 0.38 with round jets (Re = 6000–20,000). In this study, they only investigated the flow structures. Just like Kornblum and Goldstein, they demonstrated that the free jet is strongly affected by the flow exiting the concave surface. Moreover, flow visualisations show that jet vortex structures break more rapidly with increasing curvature.

Other authors have worked on more complex configurations of jets impinging on a curved surface. Bunker and Metzger (1990) studied the impingement of jets on large-scale models of the turbine blade leading edge region without variation of relative diameter. A row of jets (with 2 jet-to-jet spacing) and a slot jet were used successively and authors showed heat transfer performance to be degraded for the slot jets.

A more recent study by Iacovides et al. (2005) investigated the effect of rotation on a row of non-submerged water jets impinging on a concave surface. In a stationary configuration (which is the only configuration that may be compared to the present one), they demonstrated the presence of the "fountain effect "(maximum local heat transfer between jets).

All of these studies provide valuable information about the influence of relative curvature on flow and heat transfer due to impinging jets but, except for the last one, which was limited to flow structures, none of them analysed the effect on heat transfer of high relative curvature, such as that encountered in the leading edge of turbine blades. Moreover, jet temperature was always fixed equal to the ambient one, which essentially meant that none of these studies considered the effect on heat transfer of entrainment of ambient or recirculation air into the jet. In fact, entrainment effect is generally studied with a single jet or row of jets impinging on flat plate. Hollworth and Wilson (1984), Hollworth and Gero (1985), Goldstein et al. (1990), Baughn et al. (1991) and Fénot et al. (2005) have studied this effect measuring the adiabatic wall temperature and using it as a reference temperature in their heat transfer coefficient definition. In these cases, heat transfer coefficient seems to be independent from $(T_j - T_\infty)$.

So, the present study was undertaken in order to investigate the effect of high relative curvature on heat transfer coefficient and adiabatic wall temperature that is characteristic of the entrainment into the jet. For reasons of comparison with the results of Fénot et al. (2005), the experiment was conducted with a row of round air jets from a long pipe nozzle (for a fully developed jet) impinging on a concave surface. Injection Reynolds number varied from 10,000 to 23,000, and jet exit to plate spacing (H/d) from 2 to 5. Jet-to-jet spacing (P/d) can be set to 4 or 8 and the case of a single jet ($P/d = \infty$) is likewise investigated. Those parameters (Re, H/d, P/d) have been chosen for the sake of comparison with the results of Fénot et al. (2005). Moreover, an injection Reynolds number of 23,000 is commonly used in reference studies (Baughn and Shimizu (1989) for example). The lower limit of Reynolds number range and the values of H/d and P/d have been chosen considering real parameters in a turbine blade. The relative curvature (d/D) is varied by changing tube diameter: d/D range from 0.1 to 0.2 using 10 mm, 15 mm and 20 mm tube diameters. Injection temperature can vary from ambient temperature (around 20 °C) to 60 °C.

2. Experimental apparatus

Fig. 1 is a schematic of the experimental apparatus and Fig. 2 represents the test section. The equipment is basically the same as that used by Fénot et al. (2005) aside from the impinging plate,

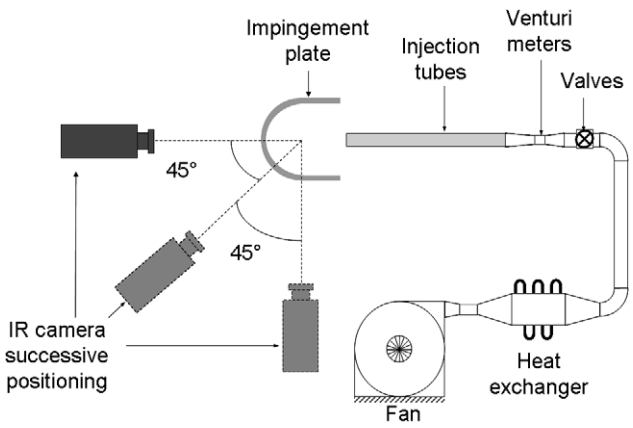

Fig. 1. Experimental apparatus.

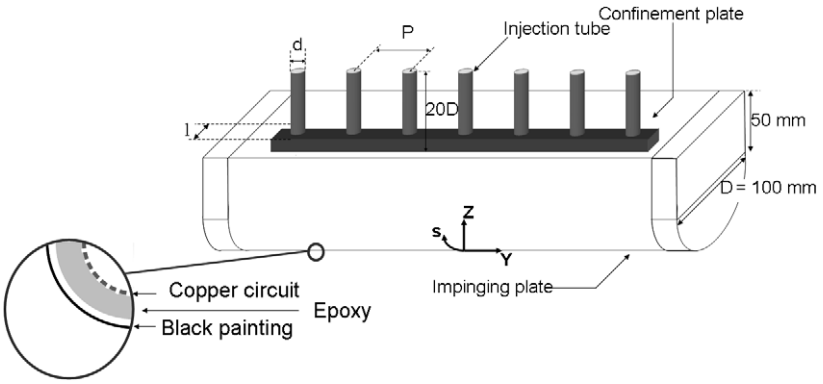

Fig. 2. Test section and impingement plate.

which is now concave. The airflow is supplied by a fan, passes through a filtration gear and enters into a heat exchanger, which enables regulation of air temperature from 15 °C to 70 °C. The flow is then divided between the different jets' respective flows. For each jet, a valve and a Venturi meter allow for control and measure of the mass flow. Venturi meters and associated pressure converters had previously been calibrated over the mass flow rate used in the experiment. Flexible conduits connect Venturi meters to injection tubes and allow variation of the jet exit to plate spacing.

As seen in Fig. 2, jets are formed from aluminium tubes. The tubes' length to diameter ratio (L/d) is 20, which is a length sufficient to obtain a fully developed exit jet flow.

The variation of relative curvature is brought about by varying the injection tubes' diameters and maintaining impingement plate diameter. Tubes with diameters of 10 mm, 15 mm and 20 mm are used for relative curvature $d/D = 0.1$, 0.15, 0.2, respectively. This methodology is consistent with other studies (Hrycak (1981), Gau and Chung (1991), Lee et al. (1999), Cornaro et al. (1999)).

Distance between injection tubes (P/d) is four times jet diameter. Variation of jet-to-jet distance (P/d) is brought about by closing half of the jets ($P/d = 8$) or by maintaining only the central jet open ($P/d = \infty$). A small confinement plate (Fig. 2) is placed at the exit of injection tube to assure a good alignment and to prevent the flow from exiting between tubes. This plate is 30 mm large and 15 mm thick. Its influence over heat transfers is small. Jet temperature is measured at the exit of the tubes using thermocouples situated in the potential core region. The temperature scattering between jets is less than 0.2 °C.

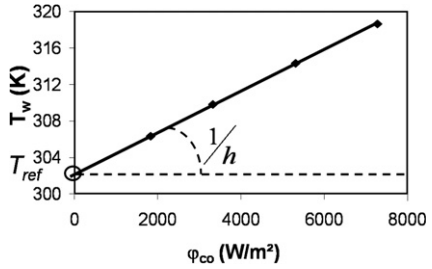

Fig. 4. Heat transfer measurement principle.

The impingement surface is a semi-cylinder of 100 mm of inner diameter prolonged by two 50 mm long flat parts. The plate is a 0.8 mm thick epoxy plate (epoxy thermal conductivity has been measured: $\lambda_w = 0.320 \pm 8 \times 10^{-3}$ W/mK with expanded uncertainty for 95% confidence level) covered with a thin foil (17.5 μm thick) of copper on its front side (side on which jets impinge). This foil is engraved by a circuit that is linked to a DC supply and allows heating of the plate by Joule effect. This circuit covers the entire impingement surface including the two flat parts. It is constituted of tight conductor tracks linked together at the extremities of the surface and separated from each other by small grooves (0.2 mm) as shown in Fig. 5.

The rear side of the impingement plate is painted in black to ensure high uniform emissivity for thermographic measurement ($\varepsilon_w = 0.95 \pm 0.02$ with expanded uncertainty for 95% confidence level).

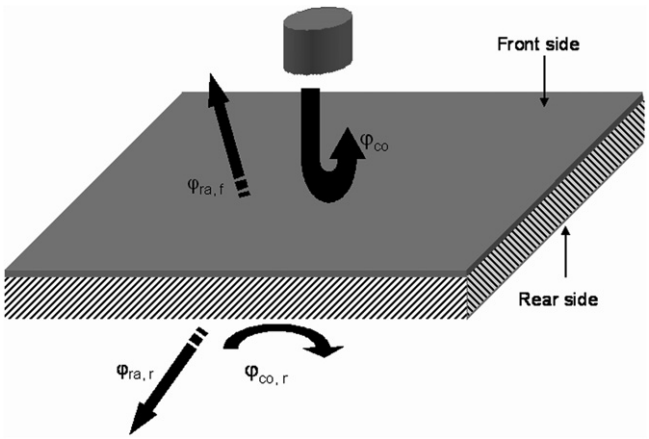

Fig. 3. Heat fluxes.

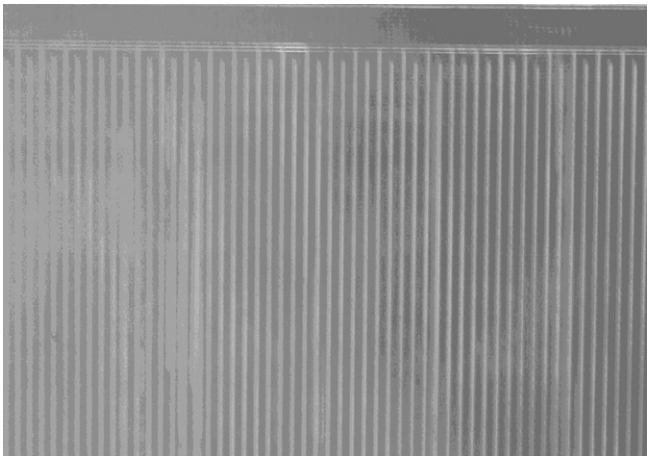

Fig. 5. Example of copper circuit.

An infrared camera (CEDIP Jade Irfpa) measures the backward temperature of the plate. Due to impingement plate curvature, three IR camera positions are needed for a complete cartography of the backward plate temperature as shown in Fig. 1. In this study, which pertains to steady state, each thermographic image is the result of the mean of 32 images recorded for 10 s. This mean allows one to remove measurement noise.

3. Heat transfer measurement procedures

The general definition of heat transfer coefficient h, also known as Newton's law of cooling is

$$h = \varphi_{co}/(T_w - T_{ref}) \tag{1}$$

This can also be written:

$$T_w = \varphi_{co}/h + T_{ref} \tag{2}$$

In Eq. (1), T_{ref} is the reference temperature depending on the configuration, and we sought out a reference temperature as heat transfer coefficient would be independent from thermal conditions. So, for different flux densities, heat transfer coefficient h should remain the same. If we inject four different convective heat flux densities and if the wall temperature T_w is measured for each one, we should have a straight line linking each couple (φ_{co}, T_w) as seen in Fig. 4. Then 1/h will be the slope and T_{ref} the y-intercept. So, T_{ref} is equal to the wall temperature when there is no exchange between the plate and the flow, which is precisely the definition of adiabatic wall temperature T_{aw}. Moreover, using this definition, the heat transfer coefficient is presumed to be independent from flux density. If it is not, then the correlation coefficient of linear regression will be far from 1.

In practice, the technique consists in electrically heating the impingement plate using copper circuits. This enables the experimenter to calculate the exact electrical flux density dissipated by Joule effect φ_{elec}. Electrical resistivity variation with temperature is taken into account in calculus of the heat fluxes. Radiative and convective losses must be calculated to obtain the convective heat flux density on the front side φ_{co}, which is an exchange between plate and jets as presented in Fig. 3:

$$\varphi_{co} = \varphi_{elec} - \varphi_{co,r} - \varphi_{ra,f} - \varphi_{ra,r} \tag{3}$$

$$\varphi_{co,r} = h_r(T_{w,r} - T_\infty) \tag{4}$$

$$\varphi_{ra,f} = \sigma\varepsilon_w\left(T_w^4 - T_j^4\right) \tag{5}$$

$$\varphi_{ra,r} = \sigma\varepsilon_w\left(T_{w,r}^4 - T_\infty^4\right) \tag{6}$$

As regards the convective heat flux density on the rear side $\varphi_{co,r}$, a heat transfer coefficient h_r has been measured during a separate experiment: all jets are cut off and the front side is isolated so that nearly all the electrical flux is dissipated on the rear side by convection or radiation. During this particular experiment, electrical flux is fixed so that the average temperature of the plate remains the same as the one in an experiment with jets turned on. Radiation flux densities are calculated as above (Eq. (6)) then, knowing the heat flux density on the rear side $\varphi_{co,r}$ and the wall rear temperature, it is possible to determine local heat transfer coefficient on the rear side h_r. As the impinging plate is positioned vertically (with gravity along the Y axis), h_r varies along with Y. At the bottom $h_r = 14$ and decreases up until a value of 8 at the top of the plate.

In the worst case, the sum of radiative and convective losses represents less than 15% of the electrical flux density, so uncertainties for these losses exert little influence over uncertainty for heat transfer coefficient and adiabatic wall temperature.

So, heat flux density on the front side φ_{co} (exchanged between the jets and the plate) varies from 4000 W/m^2 (for the smallest of the four convective heat flux densities for a given configuration) to 12,000 W/m^2 (for the greatest of the four convective heat flux densities for a given configuration).

Temperature is measured at the rear side of the plate and T_w can be deduced from $T_{w,r}$ with Eq. (7):

$$T_w = T_{w,r} + \frac{e}{\lambda_w}(\varphi_{co,r} + \varphi_{ra,r}) \tag{7}$$

The heat conduction within the impingement wall is considered one-dimensional due to the relatively homogeneous temperature of the plate and the small thickness of the copper foil (17.5 μm thick). A 3D numerical model of conduction in the impingement plate has been written and has confirmed that radial conduction is negligible.

So, the experimental scheme consists in fixing a given electrical flux density φ_{elec}, and in measuring the impinged wall rear temperature ($T_{w,r}$) by infrared thermography. Then φ_{co}, the heat flux density exchange between jets and the impingement plate, is deduced from φ_{elec}, and T_w, impinged wall front temperature, is deduced from $T_{w,r}$. This procedure is repeated three times, then, the four couples (φ_{co}, T_w) are used to perform the linear regression and to figure local heat transfer coefficient h and adiabatic wall temperature T_{aw}.

h and T_{aw} are a dimensioned as shown in Eqs. (8) and (9).

$$Nu = hd/\lambda_{air} \tag{8}$$

$$\eta = (T_{aw} - T_\infty)/(T_j - T_\infty) \tag{9}$$

Air thermal conductivity λ_{air} is calculated for the adiabatic temperature T_{aw}.

Average Nusselt number and effectiveness are calculated from local Nusselt number and effectiveness using the trapezoidal rule for integration along lines of constant Y/d (parallel to the impingement line). They are evaluated as follows:

$$\overline{Nu}(s) = \frac{1}{P/2}\int_0^{P/2} Nu(s,Y)\,dy \tag{10}$$

$$\overline{\eta}(s) = \frac{1}{P/2}\int_0^{P/2} \eta(s,Y)\,dy \tag{11}$$

As integration is brought about only along the Y axis, average Nusselt number and effectiveness continue to vary along curvilinear abscissa.

For the purpose of correlations, other average Nusselt number and effectiveness are calculated both along the Y and s axis for $0 \leqslant Y \leqslant P/2$ and $0 \leqslant s \leqslant 5d$ as follow:

$$\overline{\overline{Nu}} = \frac{1}{5d}\frac{1}{P/2}\int_0^{5d}\int_0^{P/2} Nu(s,Y)\,dy\,ds \tag{12}$$

$$\overline{\overline{\eta}} = \frac{1}{5d}\frac{1}{P/2}\int_0^{5d}\int_0^{P/2} \eta(s,Y)\,dy\,ds \tag{13}$$

Uncertainties are calculated using the statistical approach. Taking into account errors due to ambient and injection temperature, to electrical, radiative and convective fluxes, and to emissivities, random uncertainty for the Nusselt number values is no higher than 5% and that for effectiveness is no higher than 4%. Overall uncertainty for the Nusselt number values is no higher than 12% and that for effectiveness does not exceed 6%. All these uncertainty values have been reported at a 95% confidence level.

4. Results and discussion

4.1. General description

For each experimental configuration, maps of Nusselt number and effectiveness have been compiled. An example of these maps is presented in Fig. 6, for $Re = 23{,}000$, $H/d = 2$, $P/d = 4$, $d/D = 0.1$ and $(T_j - T_\infty) = 38$ °C. Small circular zones with no results (particu-

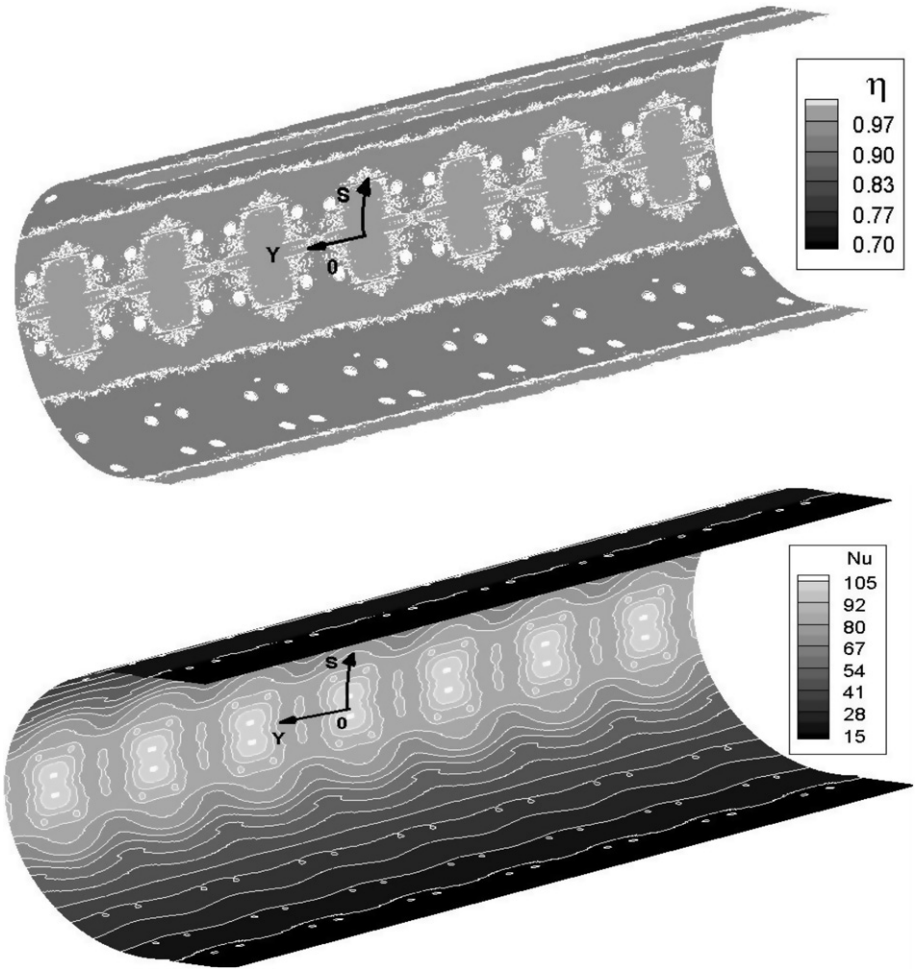

Fig. 6. Effectiveness and Nusselt number cartography (Re = 23,000, H/d = 2, P/d = 4, C_r = 0.1, $T_j - T_\infty$ = 38 °C).

larly visible on effectiveness cartography) are zones covered with the reflective adhesive used as spatial references. Even if these maps are not easy to comment, we can put forward several remarks. First of all, we can see that spanwise periodicity and symmetry are satisfactory. Therefore, later experimental results will focus on the central jet. Moreover, two lines seem particularly interesting: $s/d = 0$ along which interactions between jets should be the strongest and $Y/d = 0$ along which curvilinear effect should be dominant. The importance of these two lines is confirmed by the "eight-form" of Nusselt number maps around impinging points. Even if only one configuration is presented, these remarks are likewise valid for the others.

Since the correlation coefficient of linear regression is superior to 0.998 in all cases, the method is valid and Nusselt number is independent from wall flux density.

Fig. 7 confirms that Nusselt number calculated by the method described above is independent from the difference between jet injection temperature and ambient temperature. Adiabatic wall temperature is dependent on T_∞ and T_j but in its dimensionless form: effectiveness is independent from $(T_j - T_\infty)$ as shown on Fig. 7. Although this is illustrated for only one configuration, Nusselt number and effectiveness are independent as regards φ_{co} and $(T_j - T_\infty)$ for other configurations. So, later experimental results are presented only for $(T_j - T_\infty) \approx 40$ °C.

Since no other experiments have analysed the effect on heat transfer of high relative curvature such as those studied here, comparison of our results with those of other authors is difficult. The only possible result comparison is with Lee et al. (1999) for a single jet with an injection Reynolds number of 23,000 and an injection-to-plate distance of 2D (Fig. 8). Nevertheless, relative curvature is not exactly the same (d/D = 0.089 for Lee et al. and d/D = 0.1 for our experiment) nor is the impinging plate since the jet impinge s on a half sphere for Lee et al. and on a half cylinder for us. This second difference is particularly important as, after the impingement, the flow is axisymmetric for Lee et al.'s experiments and not for ours. This may explain the Nu differences around the impinging point. As s/d increases, differences between the two results become less sizable.

4.1.1. Effectiveness

Effectiveness distributions along $Y/d = 0$ and $s/d = 0$ are shown in Fig. 9 for Re = 10,000, 23,000 and for distance H/d = 2 and 5. The jets' impinging points are located on $s/d = 0$ and $Y/d = 0$ and 4. Whichever Reynolds number and injection-to-plate distance are considered, η remains between 0.95 and 1 at the impinging point, so adiabatic wall temperature T_{aw} is nearly equal to injection temperature. Furthermore, η is nearly constant in the two directions, a small decrease (inferior to 0.15) can be seen only along curvilinear abscissa. The stagnation of effectiveness η is due to the curvature that causes a partial confinement of the fluid. The impingement plate's flat parts reinforce this semi-confinement. In fact, the adiabatic wall temperature T_{aw} (and also effectiveness η) is linked to the temperature of the wall jet, which decreases as it mixes with ambient air. However, vortexes are created on both

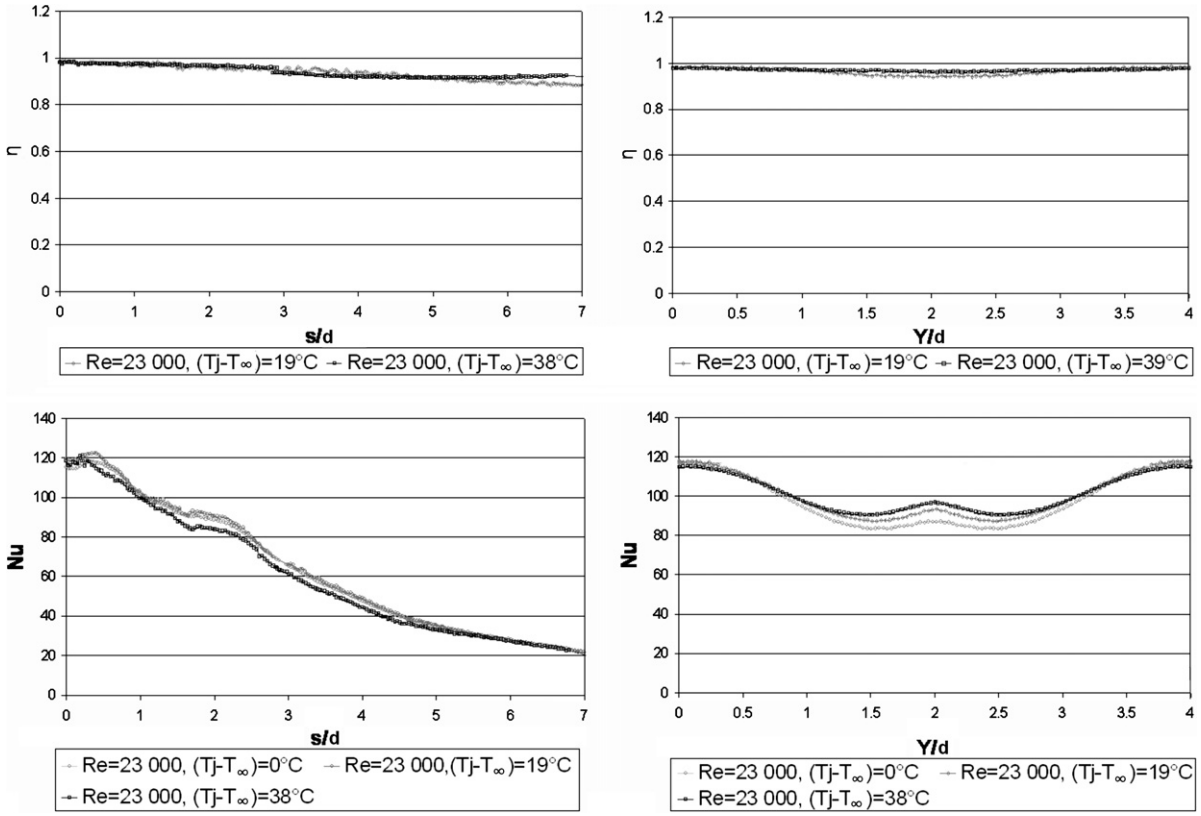

Fig. 7. Effectiveness and Nusselt number along curvilinear and longitudinal axis (Re = 23,000, H/d = 2, P/d = 4, C_r = 0.1, $T_j - T_\infty$ = 38 °C).

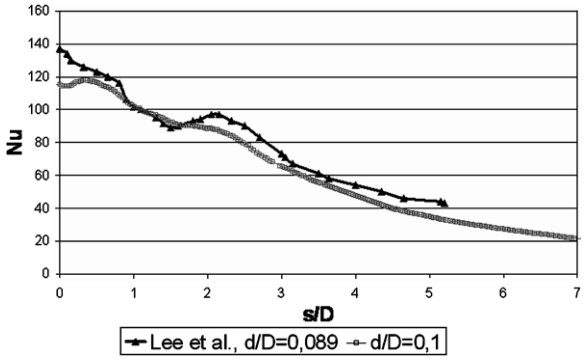

Fig. 8. Comparison with results of Lee et al. (1999) (Re = 23,000, H/d = 2, single jet).

sides of the jet, as is shown by the visualisations of Cornaro et al. (1999) and Kornblum and Goldstein (1997). These vortexes prevent the cool ambient air from mixing with jet. This "confinement" effect is increased by the flat parts of the impinging plate (Fig. 2). Furthermore, when neighbouring jets' flows meet, they go upward and two large vortexes are formed as well as smaller ones near the wall. This is called fountain effect, and it is particularly visible for $H/d = 5$ along the Y axis, where η increase around $Y = P/2 = 2$ (Fig. 9). This heightening is due to the small vortexes, which create a small recirculation zone and enhance heat transfer with the heated plate and thereby increase jet flow temperature. The two large vortexes of the fountain effect also prevent ambient air from coming close to the jets and reduce the ηdecrease even further.

For a better understanding of the curvature effect, distribution of average effectiveness (Eq. (11)) for this concave plate is compared in Fig. 10 with that of a flat plate lacking and containing a confinement plate (from Fénot et al. (2005)). The experimental apparatus used for these three configurations is nearly the same except for the impinging and confinement plates. At the impinging point line ($X/d = 0$ or $s/d = 0$), distributions are nearly identical for $H/d = 2$, whereas for a greater jet exit to plate spacing ($H/d = 5$), $\overline{\eta}$ is weaker for the flat plate without semi-confinement on account of the mixing of jets' flow with ambient air before the impact. For the curved and the semi-confined configuration, $\overline{\eta}$ is close to 1 at the impinging point line because the jets mix only with the hot air arising from the spent flow. For the same reason, average effectiveness decreases distinctly for the flat plate without semi-confinement, whereas $\overline{\eta}$ remains nearly constant for the two other configurations.

4.1.2. Nusselt number

Fig. 11 shows Nusselt number distributions for the four configurations already presented as regards effectiveness.

Oppositely to effectiveness, Nusselt number varies quite strongly with Reynolds number. For a flat plate, this dependence is generally approximated by power law dependence: Nu–Re^n, with n depending on several factors and especially distance from impinging point. By means of least square analysis, we have determined that a value of 0.65 fits the data for $s/d < 2$ and that a higher value (0.8) fits the data for $s/d > 2$. For a line of jets impinging on a flat plate with nearly the same P/d and Z/d, Goldstein and Seol (1991) have measured $n = 0.67$ for the impinging line and $n = 0.74$ for downstream location. Influence over Nusselt number of injection Reynolds number is manifestly nearly the same for a flat and a curved plate. Looking more precisely at the Nusselt number distribution along s axis, we may observe that at the impinging point, Nu is at a local minimum for Re = 23,000 (both $H/d = 2$ and $H/$

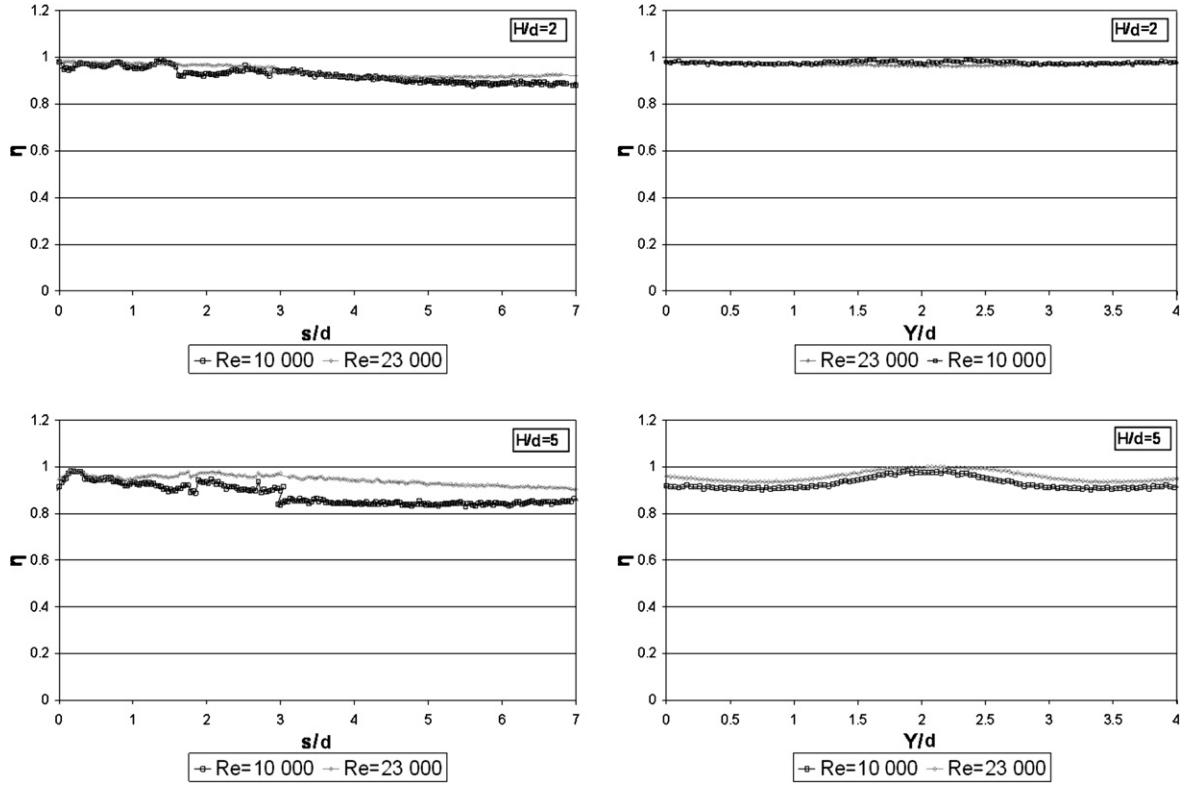

Fig. 9. Effectiveness along curvilinear and longitudinal axis ($P/d = 4$, $C_r = 0.1$).

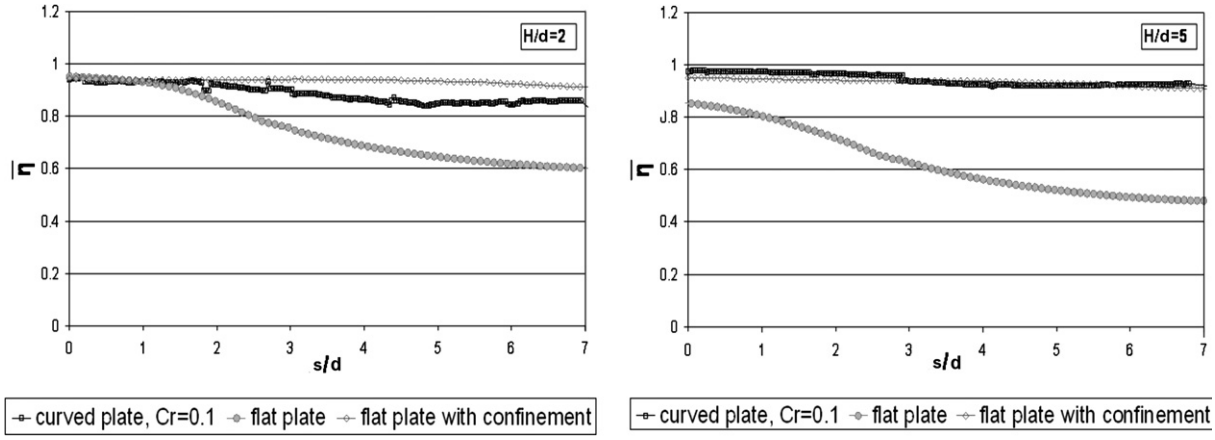

Fig. 10. Average effectiveness along curvilinear axis for flat and curved plate ($Re = 23{,}000$, $P/d = 4$).

$d = 5$), then Nu increases up to $s/d = 0.25$ for $H/d = 5$ and up to $s/d = 0.4$ for $H/d = 2$. This maximum corresponds approximately to the width of the potential core (larger for $H/d = 2$ than for $H/d = 5$). There is no such minimum for $Re = 10{,}000$, but Nu is constant up until the same s/d. No minimum is visible for an impinged flat plate with these ranges of injection Reynolds number and jet exit to plate spacing (Fénot et al. (2005)). In fact, minima are not restrained at the impinging points; there is a "Nusselt number minima line" all along the Y axis. This may be seen on Fig. 6, even if it is not clearly delineated. This minima line could correspond to a "dead fluid" area similar to the one observed by Gilard and Brizzi (2005) for a slot jet. This area could prevent jets from coming into impact with the curved wall and thereby reduce the Nusselt number at the impinging point.

For $s/d > 0.4$, Nu decreases with increasing s/d. Slope changes are visible for $s/d \approx 1.6$ and $s/d \approx 2.1$ and correspond to the local minimum and maximum encountered with jets impinging on flat plate. It seems that plate curvature reduces the "intensity" of these extremes. Two theories are generally proposed to explain local maximum: the first is that it is caused by the transition from a laminar to a turbulent boundary layer, the second that it is caused by breaking of coherent vortices close to the plate surface. Whichever theory is considered, it would seem that plate curvature perturbs the near wall flow because of the centrifugal forces that may destabilize the flow as pointed out by Gau and Chung (1991).

Along the Y axis, Nu distributions of concave and flat plate present the same variation: Nu decreases until $Y/d = 1.5$, then it increases for $Re = 23{,}000$ and $H/d = 2$ and remains constant for the

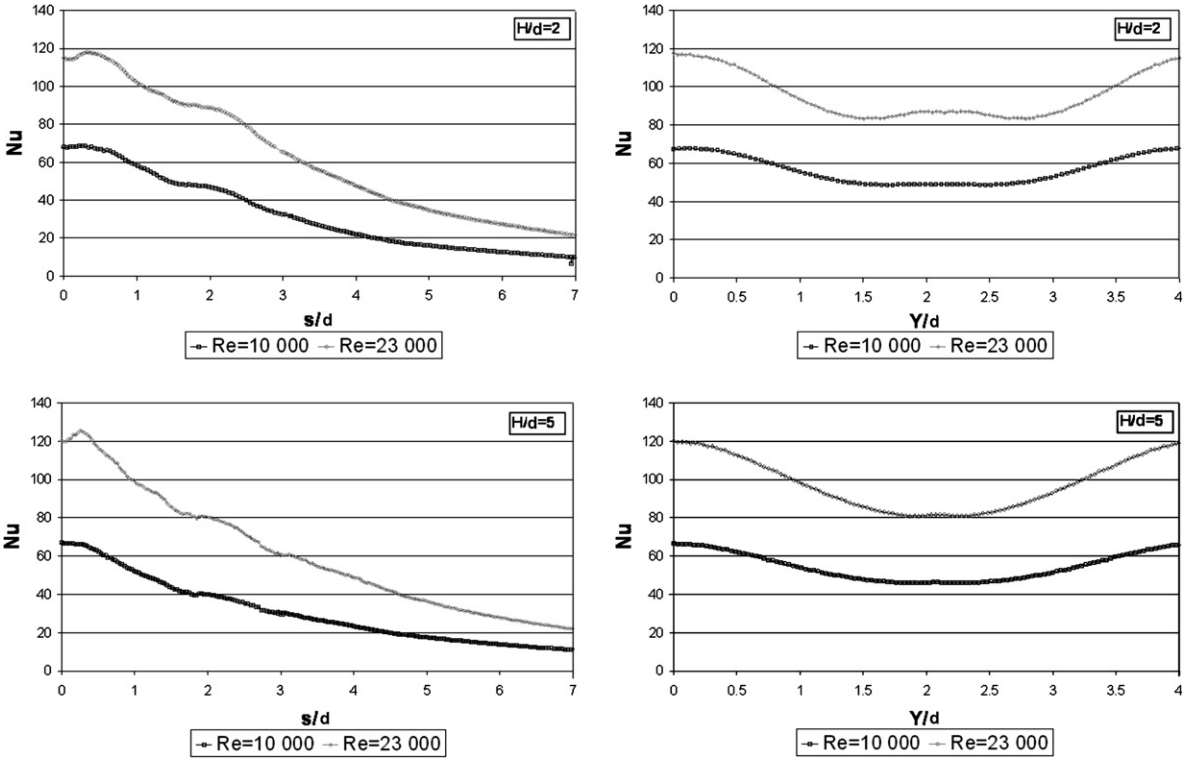

Fig. 11. Nusselt number along curvilinear and longitudinal axis ($P/d = 4$, $C_r = 0.1$).

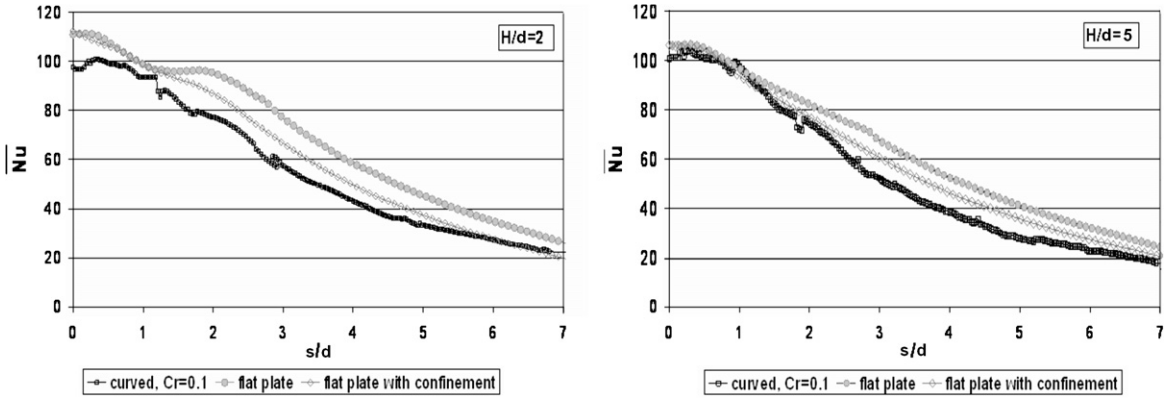

Fig. 12. Average Nusselt number along curvilinear axis for flat and curved plate ($Re = 23{,}000$, $P/d = 4$).

other configurations until $Y/d = 2 = P/2$. After that, the distribution is symmetrical. The local maximum at $Y/d = 2$ is due to the fountain effect as regards effectiveness.

Fig. 12 presents distributions of average Nusselt number (Eq. (10)) for curved plate and flat plate with and without semi-confinement. Throughout the plate, Nusselt number is lower for the curved plate than for the flat plate. Except for $H/d = 2$, the relative difference is small up until $s/d = 1.5$ and increases afterwards. The difference between the curved plate and the flat plate with semi-confinement is less pronounced. These results are surprising insofar as concave surface is generally presumed to enhance Nusselt number as shown by Gau and Chung (1991) or Lee et al. (1999) (also see *curvature effects* below). That said, a rather similar observation was voiced by Kornblum and Goldstein (1997) when they compared impingement on concave and convex surfaces. It is worth noting that Gau and Chung (1991) and Lee et al. (1999) worked with small relative curvatures (between 0.01 and 0.09) and consequently with a smaller confinement effect. Moreover, they did not compare their results with a flat plate. As $\overline{Nu}$ is likewise reduced for a flat plate with semi-confinement, the confinement effect due to the concave surface is probably partially responsible for the $\overline{Nu}$ reduction on the curved plate. The perturbation of jets by the spent flow is another possible cause, and it was proposed by Kornblum and Goldstein (1997). These two explanations can be linked insofar as semi-confinement can induce the fountain effect flow to perturb jets, even with a flat plate.

4.2. Jet to jet spacing effects

Fig. 13 shows examples of effectiveness distribution along s and Y axis for several jet-to-jet distances. Only configurations with injection Reynolds number of 23,000 are presented but all remarks

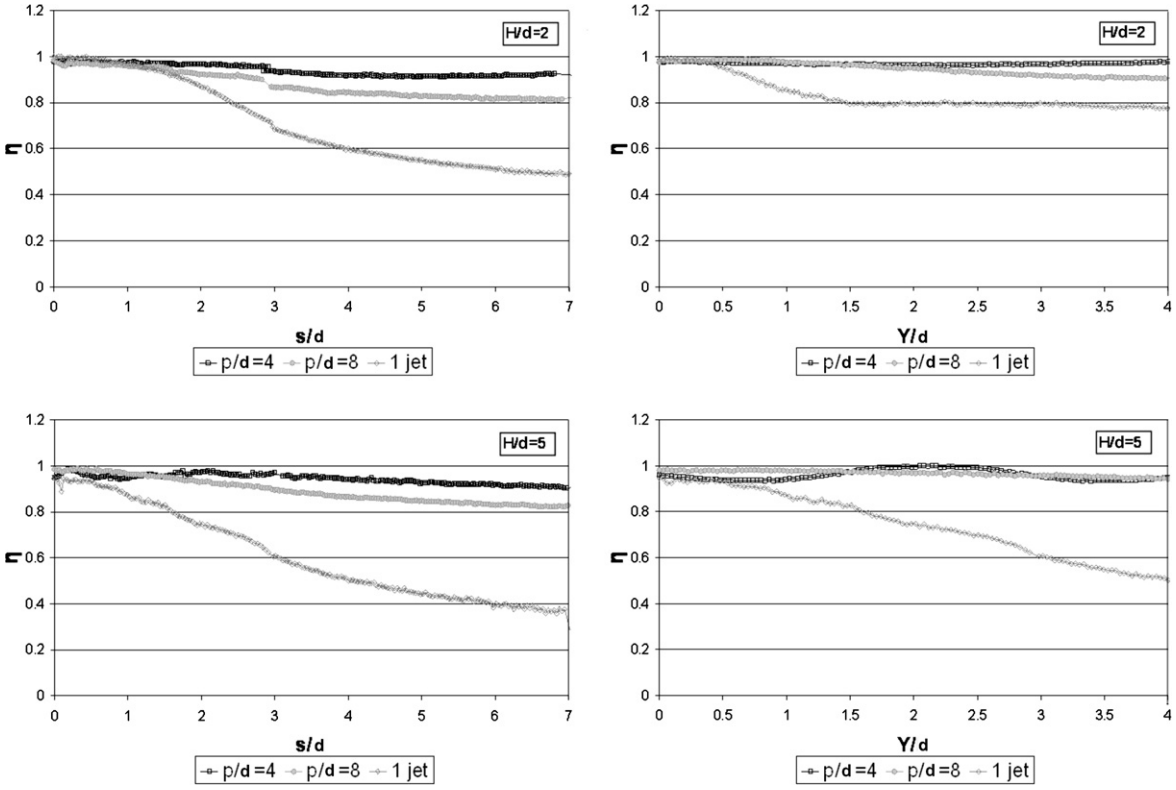

Fig. 13. Effectiveness along s and Y axis for 3 jet-to-jet spacing (Re = 23,000, C_r = 0.1).

remain valid for configurations with another Reynolds number. Three configurations have been studied: $P/d = 4$, $P/d = 8$ and a single jet which corresponds to the limit situation of $P/d = \infty$.

At the impinging point, η is nearly the same for all configurations. Even for the single jet, the "confinement" effect of the curvature prevents the injection temperature from decreasing before the impact. By moving away from the impinging point, η curves move away from each other: effectiveness decreases more rapidly when P/d is greater. As this is particularly obvious for one jet, the fountain effect seems to have a preponderant role over both the temperature of the jet and effectiveness. When P/d increases, the fountain effect is less intense, vortexes are smaller and cool ambient air can mix with hot jet flow and reduces its temperature. The effectiveness decrease is more pronounced for $H/d = 5$ since the interaction zone between jets and ambient air is larger for greater injection-to-plate distance.

Effectiveness distribution is not axisymmetric for the single jet: η decreases more rapidly along the s axis than along the Y axis. This is quite logical insofar as the effectiveness decrease is due to jet mixing with ambient air, and only with difficulty can ambient air reach the Y axis at the bottom of the impinging plate.

Nusselt number distributions are presented on Fig. 14 for the same configurations. Along the curvilinear abscissa, Nu varies little with P/d. On $Y/d = 0$ the effect of the neighbouring jets is non-existent. Along the Y axis, the three curves are very close to each other up until $Y/d \approx 1.5$–2, and the curve for $P/d = 4$ rises because of the fountain effect and then becomes the symmetric to the first part, whereas the other two continue to drop. Nusselt number enhancement due to the fountain effect is no longer visible for $P/d = 8$. Nu becomes constant after $Y/d = 3.8$: neighbouring jets are too far away to increase heat transfer rate. For $H/d = 2$, Nusselt number distributions for $P/d = 8$ and 1 jet have a local "maxima" around $Y/d = 2.1$. While it is no more than a slope change for $P/d = 8$, it is a real maximum for 1-jet distribution. The single jet distribution maximum along the Y axis is much more marked than along the s axis. In fact along the Y axis the Nusselt number variation is nearly the same as on a flat plate. This similarity is normal since in the Y direction, the impingement plate is flat. The finding confirms that curvature exerts influence on the creation of the local maximum of heat transfer.

4.3. Curvature effects

Most of the data for relative curvatures of 0.15 and 0.2 were taken for an injection Reynolds number of about 10,000. As relative curvature mainly influences distributions along the curvilinear abscissa, average effectiveness and average Nusselt number distributions are the clearest way to observe its effects.

Fig. 15 presents average effectiveness for three different relative curvatures. Distributions are very close to each other. In fact, η is nearly constant and close to 1 due to the semi-confinement caused by curvature. This confinement effect is probably reduced with decreasing relative curvature. However, since the three curvatures studied here are relatively high, and η is nearly equal to 1, the decreasing effect is not perceptible (see Fig. 16).

Nor is curvature effect over Nu highly pronounced. Moreover, this effect depends on the region: around the impinging point, $\overline{Nu}$ increases slightly with increased relative curvature. For greater curvilinear abscissa, this increase is less and less pronounced. And finally, for $s/d > 2$ or 2.5, $\overline{Nu}$ decrease with increasing C_r. The length of these two regions depends on the injection-to-plate distance: the three different C_r distributions cross each other at $s/d = 1.8$ for $H/d = 2$ and at $S/d = 2.3$ for $H/d = 5$. These results seem in contradiction with those presented above since $\overline{Nu}$ distributions are lower for a concave than for a flat one, which corresponds to a plate with $C_r = 0$. In fact, this apparent contradiction is probably due to two opposed effects: the "confinement" effect that reduces the heat transfer, and the "concavity" effect that enhances it. We have

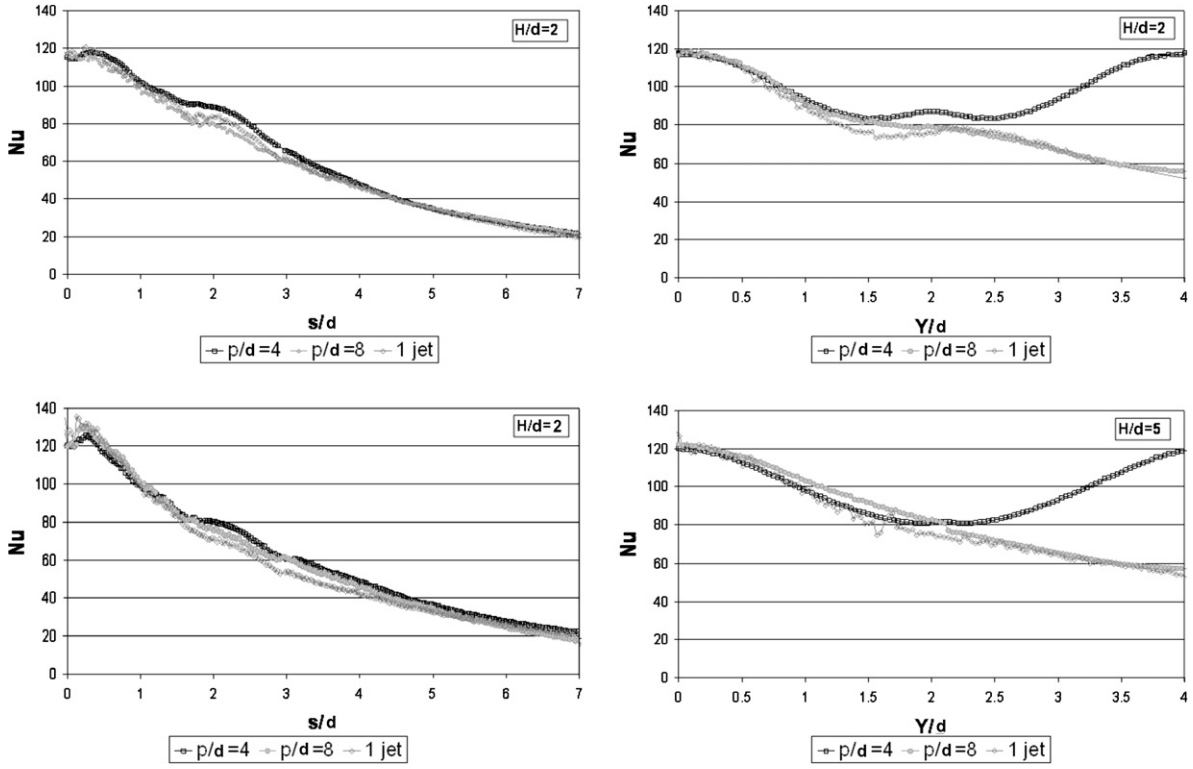

Fig. 14. Nusselt number along s and Y axis for 3 jet-to-jet spacing (Re = 23,000, C_r = 0.1).

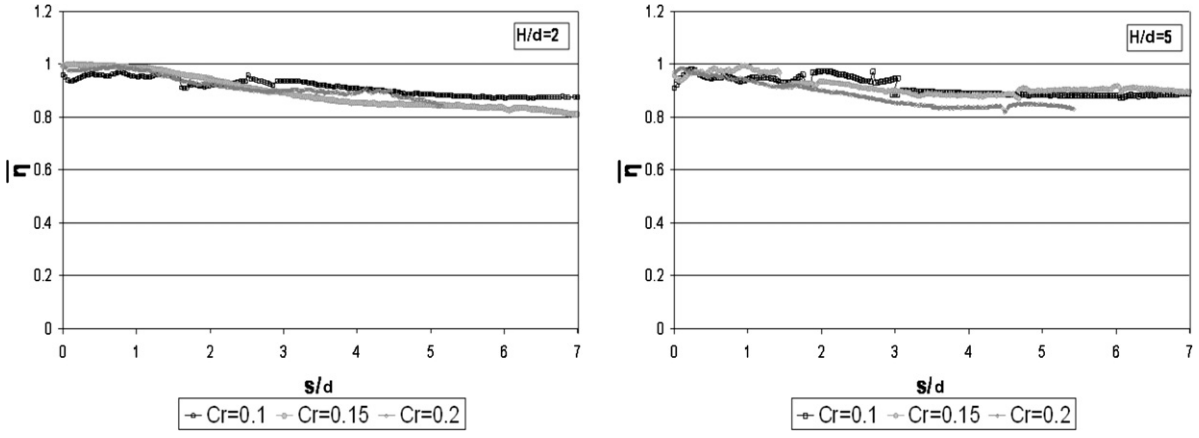

Fig. 15. Average effectiveness along curvilinear axis for various relative curvatures (Re = 10,000, P/d = 4).

already discussed the confinement effect comparing $\overline{Nu}$ for flat plate with and without semi-confinement and have concluded that the confinement reduces heat transfers. That is why $\overline{Nu}$ is higher for the flat plate without confinement than for the curved plate with which the concavity of the impingement plate produces a sort of confinement. But the confinement effect does not seem to be heightened with increasing curvature, as η, which is quite sensitive to confinement effect, is the same for the three curvatures. So, differences between the three $\overline{Nu}$ distributions are probably due to the second effect.

This second effect has been noted by other authors such as Gau and Chung (1991) and Lee et al. (1999). Several possible causes were hypothesised: thinning of boundary layer and appearance of Taylor Gortler vortices due to centrifugal forces but with no proof or visualisation.

4.4. Correlations

Correlations of stagnation Nusselt number (Nu_{st}) and effectiveness (η_{st}) in terms of injection Reynolds number (Re), injection-to plate distance (H/d) and relative curvature (d/D) are obtained as follows:

$$Nu_{st} = 0.18 \times (Re)^{0.69} \times (H/d)^{0.09}(d/D)^{0.24} \quad (14)$$

$$\eta_{st} = (H/d)^{-0.03} \quad (15)$$

The above correlations are valid for $10{,}000 \leqslant Re \leqslant 23{,}000$, $2 \leqslant H/d \leqslant 5$ and $0.1 \leqslant d/D \leqslant 0.2$.

Concerning the first correlation, Nu_{st} varies according to $(d/D)^{0.24}$ which approximately agrees with the results of Lee et al. (1999). For the effectiveness at stagnation point, the only factor that seems to have a little influence over it is the H/d.

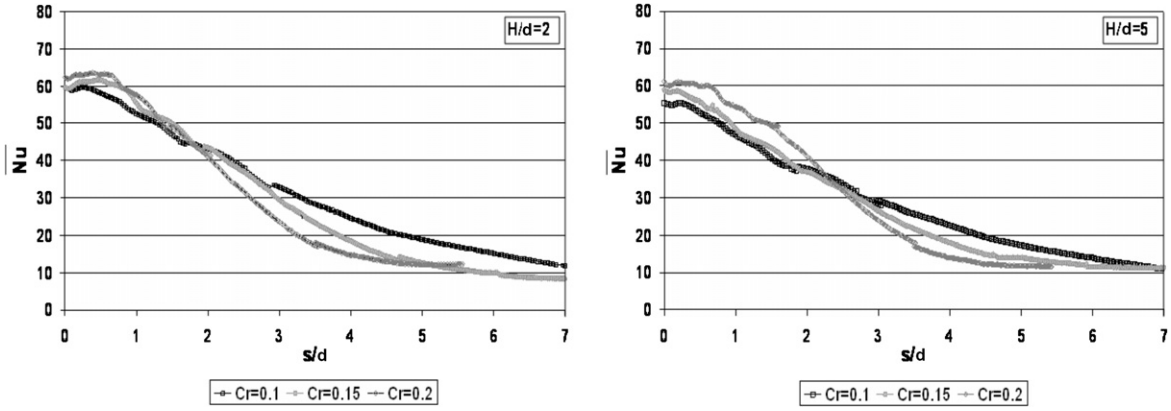

Fig. 16. Average Nusselt number along curvilinear axis for various relative curvatures (Re = 10,000, P/d = 4).

Difference between the correlation value mentioned above and our results is inferior to 2.6% for Nu_{st}, and to 1% for η_{st}.

Correlations of average Nusselt number ($\overline{\overline{Nu}}$) and average effectiveness ($\overline{\overline{\eta}}$) in terms of Re, H/d, d/D are obtained as follows:

$$\overline{\overline{Nu}} = \frac{1}{5d}\frac{1}{P/2}\int_0^{5d}\int_0^{P/2} Nu(s,Y)\,\mathrm{d}y\,\mathrm{d}s = 0.042 \times (Re)^{0.72} \times (H/d)^{-0.06}(d/D)^{-0.085} \quad (16)$$

$$\overline{\overline{\eta}} = \frac{1}{5d}\frac{1}{P/2}\int_0^{5d}\int_0^{P/2} \eta(s,Y)\,\mathrm{d}y\,\mathrm{d}s = 0.087 \times (H/d)^{-0.03}(d/D)^{-0.037} \quad (17)$$

The above correlations are valid for $10{,}000 \leqslant Re \leqslant 23{,}000$, $2 \leqslant H/d \leqslant 5$ and $0.1 \leqslant d/D \leqslant 0.2$.

Difference between average Nusselt and effectiveness correlations value and our results is inferior to 3% for $\overline{\overline{Nu}}$, and to 1.5% for $\overline{\overline{\eta}}$.

5. Summary and conclusions

Heat transfer due to a row of hot jets impinging on a concave surface has been studied experimentally by measuring local Nusselt number and adiabatic wall temperature (presented on its dimensionless form: effectiveness). Effects of jet-to-jet spacing and relative curvature have likewise been studied. Comparison with a previous study presenting a relatively similar configuration (Lee et al. (1999)) shows good agreement between our results and those of Lee et al. Correlations of effectiveness and Nusselt number at stagnation points and over the whole plate have been deduced from our results.

As expected, Nusselt number Nu and effectiveness η are independent from $(T_j - T_\infty)$. η is also nearly constant and equal to 1 and adiabatic wall temperature is consequently constant and equal to injection temperature. Comparison with flat plate with and without confinement proves that the stagnation of η is due to the confinement effect caused by the high relative concavity of the impinging surface. This confinement effect prevents cold ambient air from mixing with hot jet air and thereby reducing flow temperature. Fountain effect, due to the meeting of neighbouring jets, also prevents jet cooling, as η decreases more rapidly with increasing jet-to-jet distance (and thereby decreasing fountain effect). Moreover, it seems that following a particular relative curvature, the confinement effect of the concave surface becomes constant since effectiveness distribution is equal for the three different relative curvatures (0.1, 0.15, and 0.2).

Nusselt number distribution for a concave surface resembles such distribution over a flat plate except for local minima along the impinging line and the lack of local extremes for $s/d \approx 2$. Local minima situated just in front of the injection could be the results of a "dead fluid" area that prevent jets from coming into impact. Lack of local minima around $s/d = 1.4$ and of local maxima around $s/d = 2.1$ are probably due to centrifugal forces that perturb flow of the boundary layer. More precisely, single jet Nusselt number distribution presents these extremes along the Y axis (where the plate corresponds to a flat plate) but not along the curvilinear abscissa. This finding confirms the hypothesis that concavity provokes the decrease of these local extremes. Lastly, relative curvature seems to have two opposite effects over the Nusselt number distributions. The first involves overall reduction of the Nusselt number. Since Nu is also reduced for a semi-confined flat plate, this effect is probably of the confinement variety. As for the second effect, it enhances heat transfer near the impinging zone and is probably directly due to the increase in relative curvature.

References

Baughn, J.W., Hechanova, A.E., Yan, X., 1991. An experimental study of entrainment effects on the heat transfer from a flat surface to a heated circular impinging jet. J. Heat Transfer 113, 1023–1025.

Baughn, J.W., Shimizu, S., 1989. Heat transfer measurements from a surface with uniform heat flux and an impinging jet. Trans. ASME 111, 1096–1098.

Bunker, R.S., Metzger, D.E., 1990. Local heat transfer in internally cooled turbine airfoil leading edge regions: Part I-impingement cooling without coolant extraction. J. Turbomachinery 112, 451–458.

Cornaro, C., Fleischer, A.S., Goldstein, R.J., 1999. Flow visualization of a round jet impinging on cylindrical surfaces. Exp. Thermal Fluid Sci. 20, 66–78.

Downs, S.J., James, E.H., 1987. Jet impingement heat transfer – a literature survey, ASME 87 HT 35, The National Heat Transfer Conference, Pittsburgh, Pennsylvania.

Eren, H., Celik, N., Yesilata, B., 2006. Nonlinear flow and heat transfer dynamics of a slot jet impinging on a slightly curved concave surface. Int. Commun. Heat Mass Transfer 33 (3), 364–371.

Fénot, M., Vullierme, J.-J., Dorignac, E., 2005. Local heat transfer due to several configurations of circular air jets impinging on a flat plate with and without semi-confinement. Int. J. Thermal Sci. 44 (7), 665–675.

Gau, C., Chung, C.M., 1991. Surface curvature effect on slot-air-jet impingement cooling flow and heat transfer process. J. Heat Transfer 113, 858–864.

Gilard, V., Brizzi, L.-E., 2005. Slot jet impinging on a concave curved wall. J. Fluids Eng. 127 (3), 595–603.

Goldstein, R.J., Sobolik, K.A., Seol, W.S., 1990. Effect of entrainment on the heat transfer to a heated circular air jet impinging on a flat surface. Trans. ASME 112, 608–611.

Goldstein, R.J., Seol, W.S., 1991. Heat transfer to a row of impinging circular air, jets including the effect of entrainment. Int. J. Heat Mass Transfer 34 (8), 2133–2147.

Hollworth, B.R., Wilson, S.I., 1984. Entrainment effects on impingement heat transfer: Part I: measurements of heated jet velocity and recovery temperatures on target surface. Heat Transfer 106, 797–803.

Hollworth, B.R., Gero, L.R., 1985. Entrainment effects on impingement heat transfer: Part II: local heat transfer measurements. Trans. ASME 107, 910–915.

Hrycak, P., 1981. Heat transfer from a row of jets impinging on concave semi-cylindrical surfaces. Int. J. Heat Mass Transfer 24, 407–419.

Iacovides, H., Kounadis, D., Launder, B.E., Jiankang, Li, Zeyuan, Xu, 2005. Experimental study of the flow and thermal development of a row of cooling jets impinging on a rotating concave surface. J. Turbomachinery 127, 222–229.

Jambunathan, J.E., Moss, M.A., Button, B.L., 1992. A review of heat transfer data for single circular jet impingement. Int. J. Heat Fluid Flow 13 (2), 106–115.

Kornblum, Y., Goldstein, R.J., 1997. Jet impingement on semicircular concave and convex surfaces – Part 2: Heat transfer. The Physics of Heat Transfer in Boiling and Condensation: International Symposium, Moscow, pp. 597–602.

Lee, D.H., Chung, Y.S., Won, S.Y., 1999. The effect of concave surface curvature on heat transfer from a fully developed round impinging jet. IJHMT – Technical Note 42 (13), 2489–2497.

Martin, H., 1977. Heat and mass transfer between impinging gas jets and solid surfaces. Adv. Heat Transfer 13, 1–60.

Metzger, D., Yamashita, T., Jenkins, C., 1969. Impingement cooling of concave surfaces with lines of circular air jets. J. Eng. Power 91, 149–158.

Viskanta, R., 1993. Heat transfer to impinging isothermal gas and flame jets. Exp. Thermal Fluid Sci. 6, 111–134.

Yang, G., Choi, M., Lee, J.S., 1999. An experimental study of slot jet impingement cooling on concave surface: effects of nozzle configuration and curvature. Int. J. Heat Mass Transfer 42, 2199–2209.